Steel and Composite Structures, *Vol. 22, No. 4 (2016) 797-820*
DOI: http://dx.doi.org/10.12989/scs.2016.22.4.797

Numerical analysis and horizontal bearing capacity of steel reinforced recycled concrete columns

Hui Ma [*1], Jianyang Xue [2], Yunhe Liu [1] and Jing Dong [1]

[1] *School of Civil Engineering and Architecture, Xi'an University of Technology, Xi'an, P.R. China*
[2] *School of Civil Engineering, Xi'an University of Architecture and Technology, Xi'an, P.R. China*

(*Received June 16, 2016, Revised October 24, 2016, Accepted October 30, 2016*)

Abstract. This paper simulates the hysteretic behavior of steel reinforced recycled concrete (SRRC) columns under cyclic loads using OpenSees software. The effective fiber model and displacement-based beam-column element in OpenSees is applied to each SRRC columns. The Concrete01 material model for recycled aggregate concrete (RAC) and Steel02 material model is proposed to perform the numerical simulation of columns. The constitutive models of RAC, profile steel and rebars in columns were assigned to each fiber element. Based on the modelling method, the analytical models of SRRC columns are established. It shows that the calculated hysteresis loops of most SRRC columns agree well with the test curves. In addition, the parameter studies (i.e., strength grade of RAC, stirrups strength, steel strength and steel ratio) on seismic performance of SRRC columns were also investigated in detail by OpenSees. The calculation results of parameter analysis show that SRRC columns suffered from flexural failure has good seismic performance through the reasonable design. The ductility and bearing capacity of columns increases as the increasing magnitude of steel strength, steel ratio and stirrups strength. Although the bearing capacity of columns increases as the strength grade of RAC increases, the ductility and energy dissipation capacity decreases gradually. Based on the test and numerical results, the flexural failure mechanism of SRRC columns were analysed in detail. The computing theories of the normal section of bearing capacity for the eccentrically loaded columns were adopted to calculate the nominal bending strength of SRRC columns subjected to vertical axial force under lateral cyclic loads. The calculation formulas of horizontal bearing capacity for SRRC columns were proposed based on their nominal bending strength.

Keywords: steel reinforced recycled concrete (SRRC); Columns; OpenSees software; Numerical analysis; Flexural failure; Horizontal bearing capacity

1. Introduction

Recycled aggregate concrete (RAC) as a new type of construction material is used to completely or partially replace the natural coarse aggregate (NCA) adopting recycled coarse aggregate (RCA) in concrete mixtures. RAC can minimise the exploitation of non-renewable natural resources and decrease the negatively effect of the landfill saturation. Therefore, RAC is a kind of green construction material that positively contributes to the sustainable development and ecological environment. In fact, lots of studies on the material properties of RAC have been undertaken in many countries. The typical research achievements on the mechanical properties,

*Corresponding author, Ph.D., E-mail: mahuiwell@163.com

http://www.techno-press.org/?journal=scs&subpage=6 ISSN: 1229-9367 (Print), 1598-6233 (Online)

such as the mix designs, strength, stress-strain curves, fatigue, fire resistance and durability of RAC, were reviewed and summarised detailedly (Li 2008, Tabsh and Abdelfatah 2009, Xiao *et al*. 2012a, Thomas *et al*. 2013, Kim and Yun 2013, Fathifazl *et al*. 2009a, b). In addition, numbers of investigations on the mechanical properties and design methods of structures behaviour or structural members behaviour such as beams, columns, joints, frames of reinforced recycled concrete (RRC) had been also performed worldwide (Li 2009, Fathifazl *et al*. 2011, Won and Hyun 2012, Xiao *et al*. 2012b, Gonzalez and Moriconi 2014). Many results show that some mechanical properties of RAC adopting the mixture design method of conventional aggregate replacement may be inferior to those of ordinary concrete. It leads to that the bearing capacity and ductility of RRC structures or structural members are somewhat reduced to an allowable extent compared with those of ordinary reinforced concrete. On the contrary, some results (Fathifazl *et al*. 2009a, b, 2011) also indicate that RCA concrete does not lead to inferior properties when using the mixture method of Equivalent Mortar Volume. As a whole, the major conclusions of the above researches are positive and meaningful. RAC material as a green building material can be used in structural engineering through the rational designs and manufactures.

As is known to all, the steel and concrete composite structures possess a good seismic performance because they have the advantages of reinforced concrete structures and steel structures (Chitawadagi *et al*. 2010, Zhou and Liu 2010, Kim *et al*. 2011, Xue *et al*. 2012, Chen *et al*. 2015, Wang *et al*. 2015b). Composite structure as a kind of superior structure has been extensively used all over the world, particularly in the earthquake-prone regions. Due to the advantages of composite structures, some studies have began to investigate the performance of composite structures using RAC (Huang *et al*. 2012, Ma *et al*. 2013, Li *et al*. 2015, Wang *et al*. 2015a), such as steel reinforced recycled concrete (SRRC) columns and RAC-filled steel tube columns. The authors described the experimental and theoretical research on seismic performance of SRRC columns suffered from cyclic loads, which indicated that SRRC columns have good performance in terms of earthquake resistance through the reasonable design (Ma *et al*. 2013 and 2015). The previous research results obtained by the authors for SRRC columns are positive and encouraging. However, few investigations have been performed on the numerical analysis and horizontal bearing capacity of SRRC columns under cyclic loads.

In fact, the finite element analysis (FEA) or numerical simulation has gradually become a powerful tool in the research of mechanical properties for structures. It can mainly carry out the nonlinear analysis, parameter analysis and failure process analysis of structures, which makes up for the limitations of test researches. So far, ABAQUS, ANSYS and ADINA may be among the most prominent finite element analysis softwares (Xiao *et al*. 2012b, Li *et al*. 2012, Hassanein *et al*. 2015 and Talaeitaba *et al*. 2015). They have a large number of finite elements and excellent GUIs to analyze the behaviors of almost all types of structures or structural members under the different loads. However, FEA requires the large computational resources and laborious efforts. In addition, nonlinear FEA of concrete structures tend to have numerical convergence problems as well, especially under cyclic loads. It shows that FEA may not provide the most efficient solution for structural design.

Different from the above softwares, the Open System for Earthquake Engineering Simulation (OpenSees) is an open source analysis program developed at UC Berekeley and sponsored by Pacific Earthquake Engineering Research Center (Mazzoni *et al*. 2006). OpenSees has advanced capabilities for modeling and analyzing the nonlinear response of structures using a wide range of material models, rich element types, and more powerful solution algorithms. In fact, some researchers have analyzed the nonlinear behaviours and seismic responses of columns, joints,

shear walls and frames by OpenSees (Kang *et al*. 2013, Moridani and Zarfam 2013, Denavit and Hajjar 2014, Lu *et al*. 2015). It shows that the calculation results which using this software is more accurate and the computational time was reduced considerably compared with the traditional FEA softwares. OpenSees has been developed to provide an advanced computational tool for simulating the mechanical properties of structures and structural members subjected to different loads, especially seismic excitation.

Therefore, for the sake of having insight into seismic performance of SRRC columns under cyclic loads, the present work is about to use OpenSees to simulate the hysteretic behavior of columns suffered from flexural failure. The calculated hysteretic loops and skeleton curves can be obtained through the numerical analysis. After verifying the validity of the calculation results compared with the test results, parameter studies (i.e., strength grade of RAC, stirrups strength, steel strength and steel ratio) on seismic performance of SRRC columns were also performed using OpenSees in this paper. Based on the test and numerical results, a design method is adopted to calculate the horizontal bearing capacity of SRRC columns suffered flexural failure. The research conclusions can provide a theoretical reference for the seismic design of SRRC columns.

2. Analytical modeling of SRRC columns

2.1 Descriptions of specimens for SRRC columns

The seismic performance of SRRC9-SRRC17 columns under cyclic loads was investigated in detail by the authors (Ma *et al*. 2013, 2015). The geometry and reinforcements of SRRC columns was described in Fig.1. The test parameters of SRRC columns are the RCA replacement percentage, axial compression ratio, shear span ratio and stirrups ratio, as shown Table 1. All the columns were reinforced with profile steel, four longitudinal rebars and reinforced transversely with stirrups. No. 14 I-steel of Q235 was adopted and HRB335 ribbed rebar was also used for the stirrups and longitudinal reinforcements. The thicknesses of RAC cover to the outside surface of

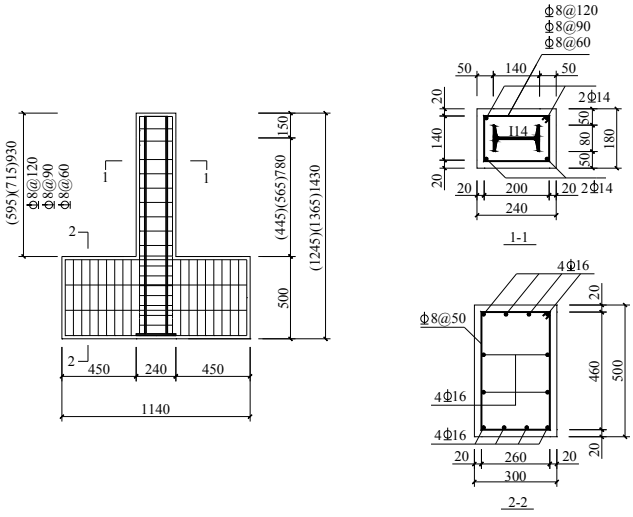

Fig. 1 Geometry and reinforcements of SRRC columns

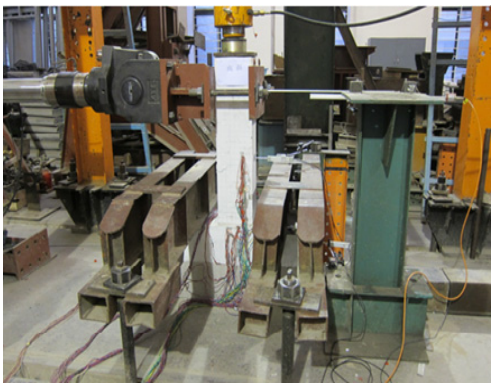

Fig. 2 Cyclic loading tests of SRRC columns

steel flanges and transverse stirrups in columns were 50 mm and 20 mm, respectively.

Table 2 lists the basic mechanical properties of profile steel and rebars. In this test, the designed 28-day cube compressive strength for the RAC mixture was around 40 MPa. In addition, a small amount of water reducing agent (i.e., the amount of water reducing agent is about 1.0% of the amount of cement) was also used in the RCA concrete mixes, so as to improve the workability of green concrete. The slump value of RAC mixture was about 70 mm in the test. The basic mechanical properties of RAC material are listed in Table 3.

The above SRRC columns were subjected to axial compression force under lateral cyclic loads, as shown Fig. 2. The results show that the failure modes of SRRC columns can be classified as flexural failure under lateral cyclic loads. It indicates that SRRC columns have better seismic performance compared with RRC columns and can be feasible to employ the composite columns in the practice of structural engineering.

Table 1 Test parameters of SRRC columns

Specimen No.	H (mm)	$b \times h$ (mm×mm)	r	λ	n	ρ_{sv}	Stirrup spacing (mm)
SRRC9	445	180×240	100%	1.85	0.6	1.36%	90
SRRC10	565	180×240	100%	2.35	0.6	1.36%	90
SRRC11	780	180×240	0	3.25	0.6	1.36%	90
SRRC12	780	180×240	70%	3.25	0.6	1.36%	90
SRRC13	780	180×240	100%	3.25	0.6	1.36%	90
SRRC14	780	180×240	100%	3.25	0.3	1.36%	90
SRRC15	780	180×240	100%	3.25	0.9	1.36%	90
SRRC16	780	180×240	100%	3.25	0.6	1.02%	120
SRRC17	780	180×240	100%	3.25	0.6	2.04%	60

Table 2 Mechanical properties of profile steel and rebars

Profile steel and rebars		Yield strength (MPa)	Peak strength (MPa)	Elasticity modulus (GPa)	Yield strain ($\mu\varepsilon$)
No.14 I-steel	Steel flange	311.5	446.5	199	1565
	Steel web	325.6	474.9	198	1644
Longitudinal rebars	ϕ14	358.0	560.9	203	1764
Stirrups	ϕ8	479.9	607.0	202	2376

Table 3 Mix proportions and mechanical properties of RAC

RAC strength grade	r	Unit weight (kg/m^3)						f_{rcu} (MPa)	E_{rcu} (GPa)
		Water cement ratio	Water	Cement	Sand	NCA	RCA		
C40	0	0.44	205	466	571	1158	0	47.70	34.26
C40	70%	0.43	205	478	549	347.4	810.6	51.82	29.56
C40	100%	0.42	205	488	527	0	1158	48.89	27.32

2.2 Fiber element models

OpenSees as an open source analysis software offers a refined and effective fiber model which is adopted in this paper (Mazzoni *et al*. 2006). The main approach of fiber model is that the section of structural members is divided into some small fiber units and the matching material properties were assigned to each fiber units. The basic assumptions of fiber model are as follow: first, the deformation of cross section of structural members is plane; second, the strain of each fiber unit on the cross section is the uniaxial stress-strain state and uniform distribution. Therefore, the force-deformation relationship of the section of structural members can be calculated by the uniaxial stress-strain relation of each fiber unit; third, the bond-slip between rebars and concrete, as well as the shear strain of fiber unit are usually neglected. Obviously, the above fiber model is suitable for simulating the mechanical properties of structural members suffered from flexural failure. In addition, OpenSees also has several restoring force models, which mainly include the elastic restoring force model, plastic restoring force model, straight-line strengthened restoring force model and hysteretic restoring force model.

OpenSees program mainly offers two types of element models, including the beam-column elements and solid elements. The beam-column elements mainly consist of truss element, elastic beam element, nonlinear beam-column element and zero dimension element. The nonlinear beam-column element has adopted the inter-polation function and the numerical integration method. It indicates that the more accurate results can be obtained compared with the current method of linear difference used by other softwares. The nonlinear beam-column element is widely used in the nonlinear analysis of structures or structural members because of its characteristics. It was proved to be able to simulate the flexural behavior of concrete structures rather well (Mazzoni *et al*. 2006, Denavit *et al*. 2014). Therefore, the nonlinear beam-column element is used to hysteretic behavior of SRRC column in this paper, which is based on the approach of fiber model.

2.3 Material constitutive model

The SRRC columns are mainly consists of three materials: RAC, profile steel and rebars. Therefore, the numerical analysis of columns requires the appropriate constitutive models of the above materials, especially for the fiber elements approach where the constitutive relations of materials should be assigned to each fiber element. In other words, it is required to partition the different zones of columns according to the constitutive relations are given to them. In addition, several assumptions should be considered in this analytical model: first, the uniform distribution of compressive strain is assumed on the cross section of columns; second, the stress of the materials are calculated based on the corresponding stress-strain relations; third, the confinement effect caused by the transverse stirrups on RAC need to be considered; last, the local buckling of longitudinal rebars and profile steel is assumed in this paper.

2.3.1 Constitutive model of RAC material

It has been widely proved that the transverse stirrups confines core concrete which can increase its strength and ductility (Denavit and Hajjar 2014). Although such enhanced effect may not be significantly observed when the columns are subjected to small axial loads, it governs the behavior of those under high axial loads or cyclic loads conditions. Therefore, the constitutive relationship of concrete should consider the confinement effect of stirrups. To facilitate the calculation, it is assumed that the confinement effect of rectangular stirrups on RAC in columns is the same in this

analysis. Concrete01 material model in OpenSees is employed for defining the unconfined and confined RAC of columns, as shown in Fig. 3. The Concrete01 model is based on Kent-Scott-Park model (1971) with the degrading linear unloading/reloading stiffness according to the research work of Karsan-Jirsa (1969). The model completely ignores the tensile strength of concrete material. It can be used to define the unconfined concrete and confined concrete. The hysteresis rules of the stress-strain of Concrete01 model are described in Fig. 4.

In SRRC columns, RAC material was used to completely or partially replace NCA using RCA in concrete mixtures. Although lots of research achievements shows that the mechanical properties of RAC material (Li 2008, Tabsh and Abdelfatah 2009, Xiao *et al*. 2012b), such as the peak stress, peak strain, ultimate stress, ultimate strain and the slope of softening section of constitutive curves have some differences compared with ordinary concrete, the curve characteristics of stress-strain relationship of RAC is similar to that of ordinary concrete. In view of this, Concrete01 model can be adopted to simulate RAC material by modifying the characteristic values of the model, such as the peak stress, peak strain, ultimate strain and the curve slope and so on. In this paper, the characteristic values of RAC using Concrete01 model can be obtained according to its material tests and other test results (Xiao *et al*. 2012a).

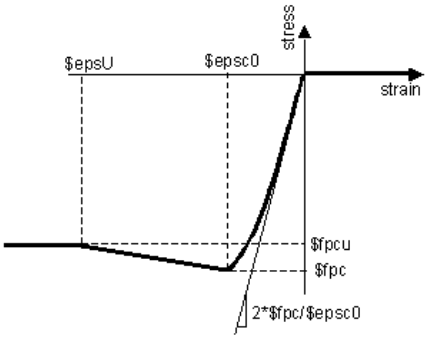

Fig. 3 Stress-strain relationship of Concrete 01 model

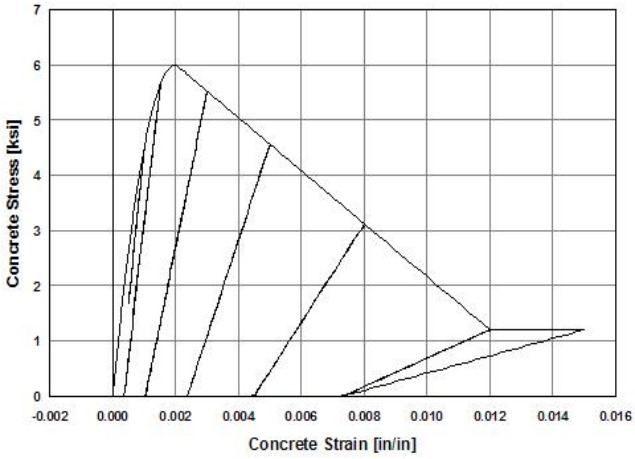

Fig. 4 Hysteretic stress-strain relation of Concrete 01 model

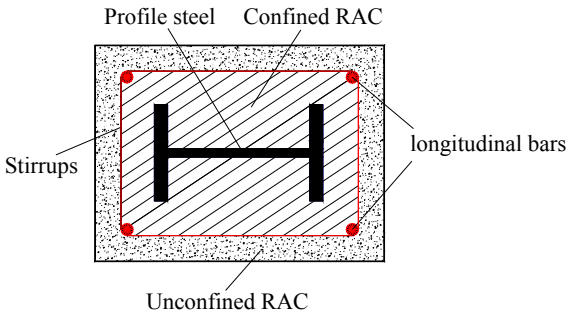

Fig. 5 Unconfined and confined RAC in SRRC columns

According to the above mentioned analysis and Fig. 5, the RAC cover of SRRC columns belongs to plain concrete, which was defined as unconfined concrete. It can directly employ Concrete01 model to simulate the plain concrete of columns. On the other hand, the confinement effect of transverse stirrups on RAC material can be determined by the formulas (1)-(6) based on Kent-Scott-Park model (1971).

$$\sigma_c = Kf_c\left[\frac{2\varepsilon_c}{\varepsilon_0} - \left(\frac{\varepsilon_c}{\varepsilon_0}\right)^2\right] \qquad \left(\varepsilon_c \le \varepsilon_0\right) \tag{1}$$

$$\sigma_c = Kf_c\left[1 - Z_m\left(\varepsilon_c - \varepsilon_0\right)\right] \ge 0.2Kf_c \quad \left(\varepsilon_c > \varepsilon_0\right) \tag{2}$$

$$\sigma_c = 0.2Kf_c \qquad \left(\varepsilon_c > \varepsilon_u\right) \tag{3}$$

$$\varepsilon_0 = 0.002K \tag{4}$$

$$K = 1 + \frac{\rho_s f_{yh}}{f_c} \tag{5}$$

$$Z_m = \frac{0.5}{\frac{3 + 0.29f_c}{145f_c - 1000} + \frac{3}{4}\rho_s\sqrt{\frac{h_c}{s_h}} - \varepsilon_0} \tag{6}$$

Where σ_c and ε_c represent the stress and strain of concrete, respectively; K is the enhancement coefficient of concrete strength due to the confinement of transverse stirrups; ε_0 is the peak strain of concrete; f_c is the compressive strength of concrete, Mpa; Z_m is the slope of softening section in the model; f_{yh} is the strength of stirrups, Mpa; ρ_s is the stirrup ratio; s_h is the spacing of stirrups; h_c is the width of core concrete surrounded by the stirrups.

2.3.2 Constitutive model of steel material

Most cases, the steel material can be usually assumed to be an elastic-perfectly plastic material. As a matter of fact, to capture the whole response of structures or structural members up to failure, the strain-hardening of steel material need to be considered in the finite element analysis. The Steel02 material model in OpenSees software, which is adopted to establish the uniaxial Giuffre-Menegotto-Pinto steel material with the isotropic strain hardening effect, is usually used to represent the nonlinear transition from elastic stage to strain hardening stage, as shown in Fig. 6. The model is bilinear which can be able to consider the effect of isotropic strain hardening and Bauschinger effect of steel material. Moreover, the yield strain of steel material can be taken as the strain hardening point according to the reference (Mazzoni *et al*. 2006). Besides, the hysteretic relationship of stress-strain for steel material was described in Fig. 7.

In this analysis, Steel02 model was adopted to describe the uniaxial stress-strain relationship of profile steel and longitudinal rebars in SRRC columns. The constitutive model of steel material is a symmetrical one, which has a same mechanical behavior in tension and compression (Mazzoni *et al*. 2006). The yield strength of Steel02 model can be obtained and confirmed through the material tests results of steel material, as shown in Table 2. The transition of the constitutive model can be adjusted manually in OpenSees by using different R_0 value. In this paper, the R_0 for the profile

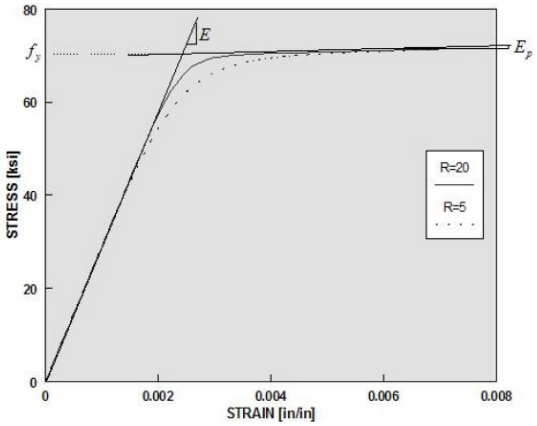

Fig. 6 Stress-strain relationship of Steel02 model

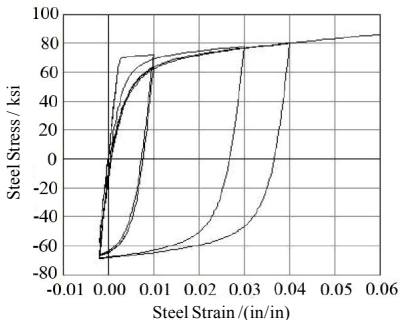

Fig. 7 Hysteretic stress-strain relation of Steel02 model

steel and longitudinal rebars was 18.5. In addition, 0.1 and 0.01 was the strain hardening rate b_1 of profile steel and rebars, respectively. C_{R2}, C_{R1} are the control coefficient of the curve shape of Steel02 model, which the values was 0.925 and 0.1, respectively.

2.4 Element division of cross sections of SRRC columns

This project employs SRRC9-SRRC17 columns as the cases, their design parameters are listed in Table 1. The displacement-based beam-column element in OpenSees was used to simulate the hysteretic behavior of SRRC columns. Fig. 8 shows the grid division of the cross sections of columns. It assumed that the columns are fixed to the ground and the columns are represented by the fiber element, as shown in Fig. 8. Along the longitudinal direction of the column, it is divided five finite elements under the lateral loads point. In each element, three integration points are

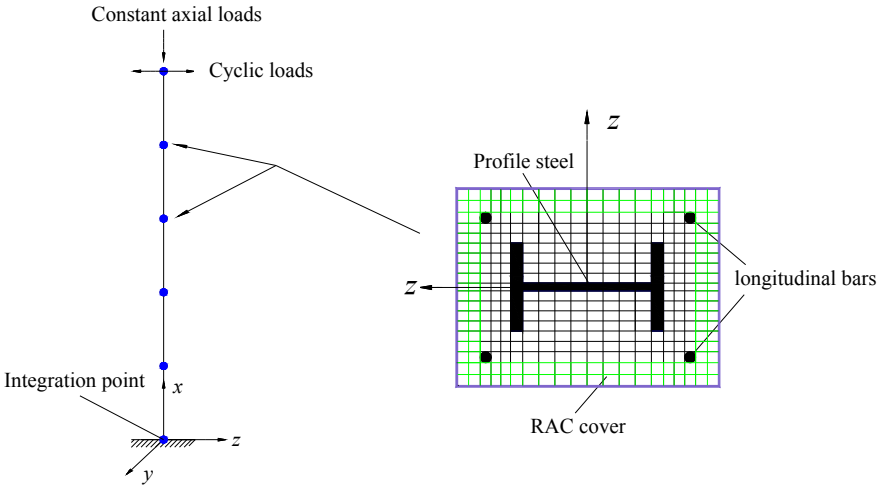

Fig. 8 Element and section division of SRRC columns

defined for calculation. The cross section of columns at each integration point is divided into several fibers to represent RAC cover, core RAC and profile steel. In the process of loading, the vertical axial load of column was finished in 10 steps and remains a constant in the analysis. There are two stages including load control and displacement control in the lateral loading process. The choice of analysis method in the calculation is Newton iterative method. Through repeated attempts to calculate, the maximum number of iterations can be identified as six times, which shows the accuracy of the calculation results meets the requirements and the calculation efficiency is relatively high by using the above computing methods. The displacement convergence criterion was adopted in the above iterative calculation. The loading process of SRRC columns would be stopped when the lateral loads reach to 85% of peak loads.

3. Comparison of test and numerical results of SRRC columns

3.1 Comparison of hysteresis loops

Based on the above models, the numerical analysis of the hysteretic behaviors for SRRC columns under lateral cyclic loads was performed in this paper. The load-displacement (P-Δ) hysteresis loops of SRRC columns were obtained according to the results of numerical analysis. The hysteresis loops mainly describe the relationship between loads and displacements on the lateral loading point of SRRC columns. Fig. 9 shows the comparison between the test and numerical hysteresis loops of SRRC columns.

From Fig. 9, it shows that the calculated hysteresis loops of SRRC columns agree well with the test curves except SRRC9 column. According to the test results, SRRC10-SRRC17 with a larger shear span ratio suffered from the typical flexural failure, which shows that the bending deformation of columns plays a decisive role in their failure process, while the shear deformation of columns can almost be ignored. The calculated hysteresis loops of SRRC10~SRRC17 columns is relatively close to the test loops, which suggests that the fiber element model in OpenSees software is suitable to simulating the hysteretic behaviors of SRRC columns suffered the flexural failure. On the other hand, the failure mode of SRRC9 column can be mainly characterized as the bending-shear failure, which is between the shear failure and the flexural failure. It shows that SRRC9 column has certain characteristics of the shear failure in its failure process. In this analysis, the fiber element model adopted in this paper has an advantage in simulating the bending deformation of columns. On the contrary, it has difficulty to analyse the effect of shear deformation of columns using the fiber model. Therefore, the calculated hysteresis loops of SRRC9 column have obvious difference compared with the test curves, due to the model almost ignores the shear deformation.

The calculated hysteresis loops of SRRC columns are spindle-shaped, which is same as the shape of test curves. The calculated curves make a better reflection on the hysteretic characteristic of SRRC columns under cyclic loads. It also shows that SRRC columns have high strength and good energy dissipation capacity under earthquake action.

3.2 Comparison of skeleton curves

The corresponding skeleton curves (P-Δ) of SRRC columns can be obtained according to the calculated hysteresis loops, as shown in Fig. 10. The skeleton curves reflect the mutual relationship between the peak loads and the corresponding displacements of columns in each

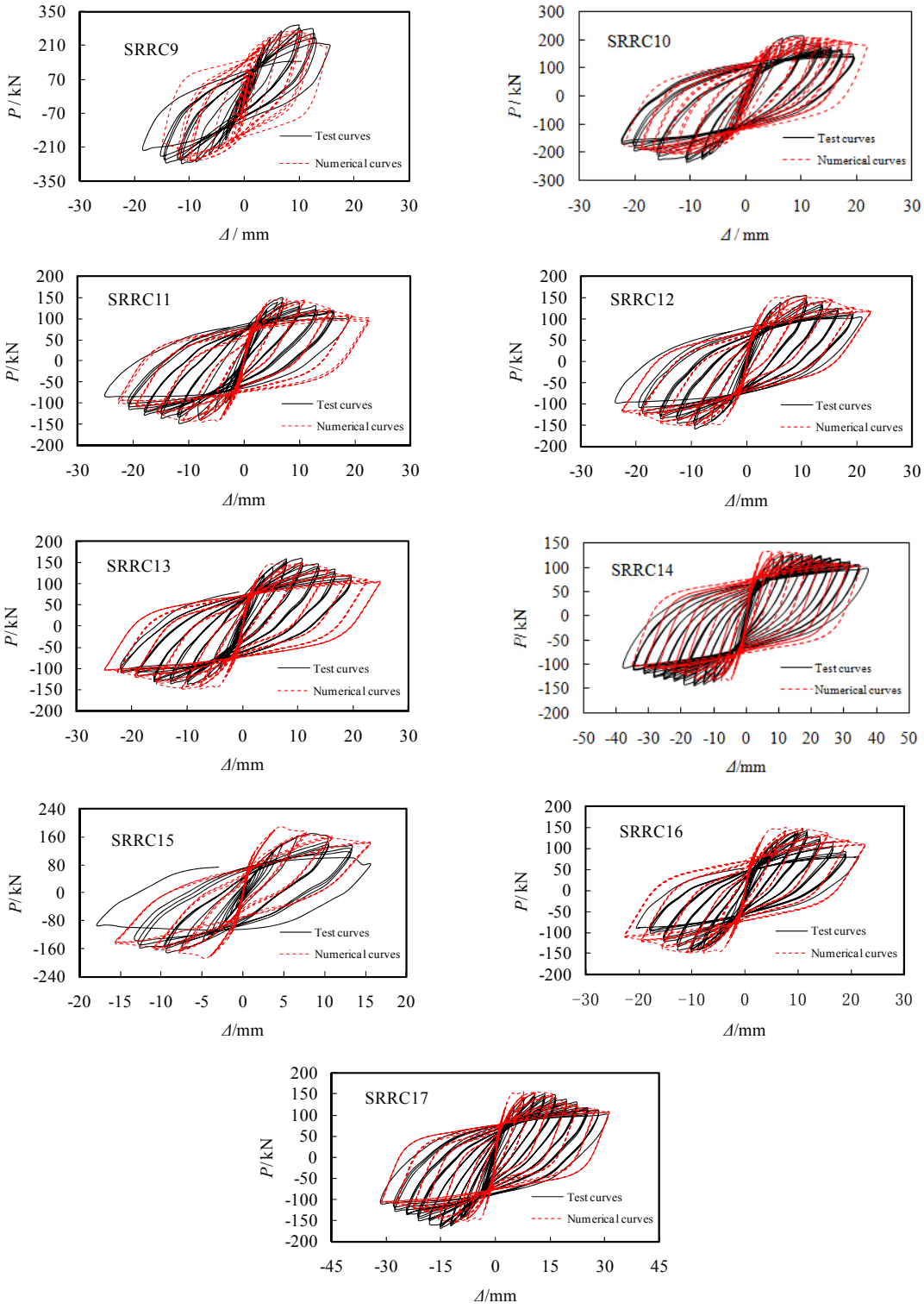

Fig. 9 Comparison between test and numerical hysteresis loops of SRRC columns

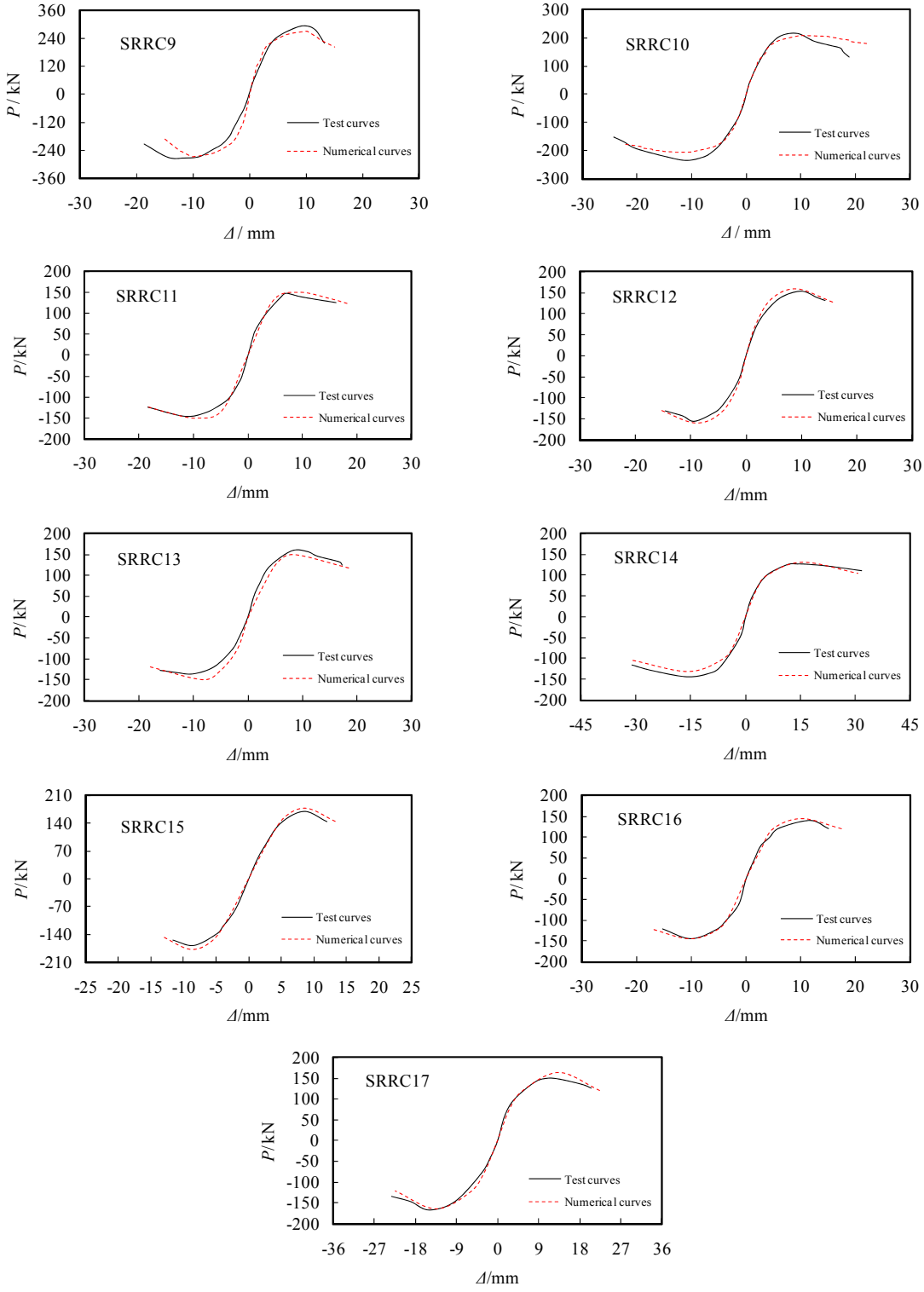

Fig. 10 Comparison of numerical and test skeleton curves for SRRC columns

Table 4 Comparison between the calculated and test results of SRRC columns

Specimen No.	r	n	λ	ρ_s	P_t/ kN	P_n/kN	δ	Failure modes
SRRC9	100%	0.6	1.85	1.36%	283.6	267.9	5.54%	Bending-shear failure
SRRC10	100%	0.6	2.35	1.36%	224.8	207.7	7.62%	Flexural failure
SRRC11	0	0.6	3.25	1.36%	146.9	149.5	1.77%	Flexural failure
SRRC12	70%	0.6	3.25	1.36%	154.6	159.6	3.23%	Flexural failure
SRRC13	100%	0.6	3.25	1.36%	147.5	149.3	1.22%	Flexural failure
SRRC14	100%	0.3	3.25	1.36%	135.7	131.4	3.17%	Flexural failure
SRRC15	100%	0.9	3.25	1.36%	168.9	178.1	5.45%	Flexural failure
SRRC16	100%	0.6	3.25	1.02%	142.4	143.7	0.91%	Flexural failure
SRRC17	100%	0.6	3.25	2.04%	158.3	164.2	3.73%	Flexural failure

loading stage. Fig. 10 describes detailedly the comparison between the calculated and test skeleton curves of SRRC columns.

From Fig. 10, the initial stiffnesses of the calculated skeleton curves of SRRC columns is close to that of the test curves, which shows the calculated skeleton curves are in good agreement with the test curves at the early stage of loading. As the increase of cyclic loads, especially after peak loads, it has some differences between the calculated and test skeleton curves, which mainly reflects in the ductile deformation and the degradation rate of bearing capacity of SRRC columns. The calculated skeleton curves of columns can be divided into the following three stages, namely the elastic stage, elastic–plastic stage and softening stage. The characteristic load points, such as the cracking point, yield point, peak point and ultimate point of columns can be obtained based on the skeleton curves. In addition, the calculated skeleton curves also show that SRRC columns have high stiffnesses and high bearing capacity under cyclic loads. The descent stage of calculated skeleton curves is relatively gentler, which indicates that SRRC columns have good ductility and deformation ability.

Based on the skeleton curves, the horizontal bearing capacity of SRRC columns can be obtained, as shown in Table 4. The error δ between the calculated and test peak loads of columns can be calculated by $\delta = |P_n - P_t|/P_t$. Based on Table 4, the calculation error of peak loads fall in between 0.91% and 7.62%. The average error of the calculated and test peak load is about 3.62%, which indicates that the numerical results are accurate and can meet the computing requirements.

The main reasons of the above error between the calculated and test peak loads of SRRC columns may be as the following: (1) the effect of bond-slip between the profile steel and RAC does not take into account in this analysis, which has a certain effect on the hysteretic behavior of columns, such as the bearing capacity, stiffness and displacement deformation; (2) the shear deformation of columns is completely ignored in this paper. In fact, the columns still has a certain shear deformation in the early stage of loading, which means that only considering the bending deformation does not comprehensively reflect the actual situation of deformation characteristics of columns; (3) the constitutive models of materials and calculation method also has some effect on the simulation results.

4. Parameters analysis on hysteretic behavior of SRRC columns

To analyze the seismic performance of SRRC columns further, the parameters analysis on the

hysteretic behavior of columns was performed using OpenSees in this paper. The simulation methods can be seen in chapter 2. Take SRRC13 column as a basis, the analysis parameters of SRRC columns are designed and listed in Table 5. The analysis parameters include the RAC strength, stirrups strength, steel strength and profile steel ratio. In this parameter analysis, the other design parameters of columns, such as the geometric sizes, RCA replacement percentage, axial compression ratio, shear span ratio and so on, are same as those of SRRC13 column.

4.1 Analysis of hysteresis loops

The load-displacement (P-Δ) hysteresis loops of the parameters analysis of SRRC columns were described in Fig. 11. The hysteresis loops show the influence rules of parameters on the hysteresis behavior of SRRC columns.

Based on Fig. 11, the influence rules of the parameters on seismic performance of SRRC columns can be described as follows:

(1) All the hysteresis loops of columns are homogeneous symmetric and plump. The shapes of the curves are very similar to the spindle, which reflects that SRRC columns have excellent energy dissipation capacity. It also shows that SRRC columns under different parameters still has good seismic performance, especially in some beneficial design parameters.
(2) As shown in Fig. 11(a), the hysteretic loops of columns became narrow gradually with the increase of RAC strength, but the phenomenon is not very obvious. Namely, the higher the RAC strength, the worse the ductility of columns. It indicates that the increasing RAC strength has an unfavorable influence on the seismic ductility of SRRC columns.
(3) The hysteresis loops of columns under different stirrups strength is almost overlapping as described in Fig. 11(b). The deformation and energy dissipation capacity of columns increase a little with the increasing stirrups strength. Although the effect on the seismic ductility of columns is not obvious, it indicates that the increased stirrups strength is still favorable to improving the seismic performance of columns.
(4) As shown in Fig. 11(c), the hysteresis loops of SRRC columns became high and narrow gradually with the increase of steel strength. The deformation and bearing capacity of columns increases gradually with the increase of steel strength. This finding indicates that the increasing steel strength can improve the seismic performance of columns. For the record, the steel strength of columns should be matching with RAC strength, to ensure the steel yield before RAC failure.
(5) The hysteresis loops of SRRC columns became plumper gradually with the increasing steel ratio, as shown in Fig. 11(d). It indicates that the deformation ability of SRRC columns increase obviously with the increased steel ratio. Besides, the attenuation of strength and stiffness of columns become slowly. It suggests that the seismic performance of SRRC columns can be improved by increasing the steel ratio.

4.2 Bearing capacity and ductility factors

The bearing capacity and ductility factors of SRRC columns can be obtained based on the hysteretic loops of parameters analysis of columns. Table 5 lists the bearing capacity and ductility factors of SRRC columns in this parameters analysis. The peak loads were taken as the bearing capacity of columns. The ductility factor μ can be calculated by $\mu = \Delta_u / \Delta_y$, which was used to

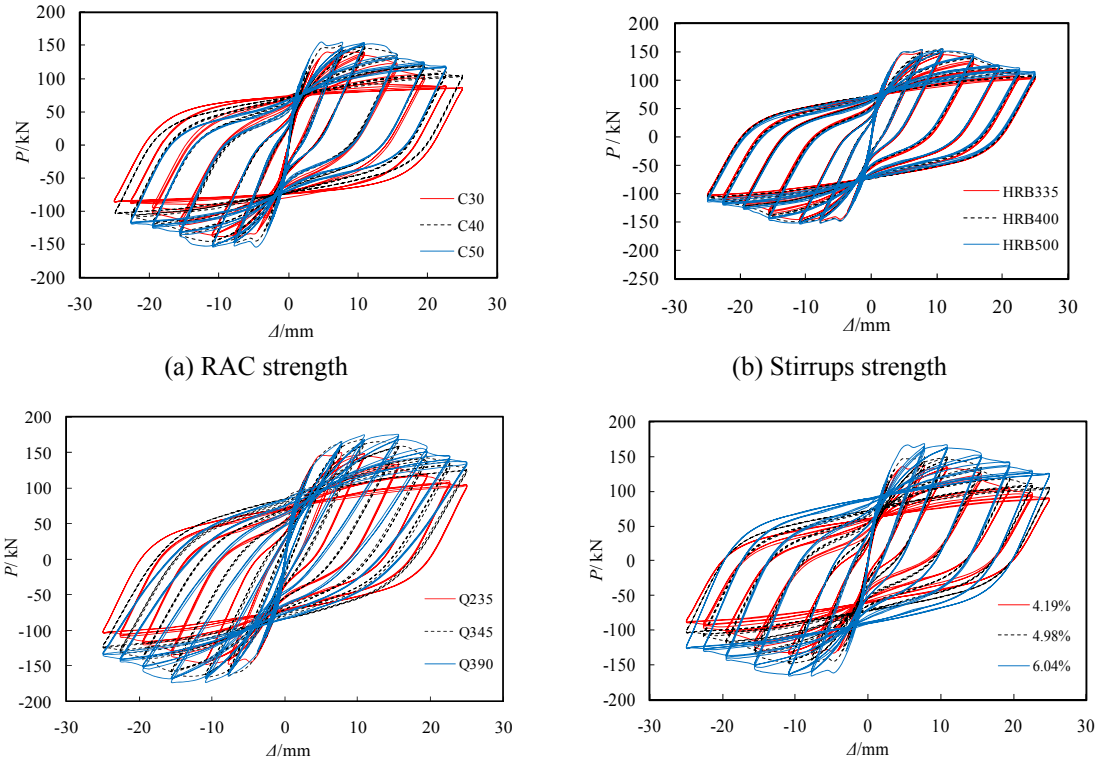

(a) RAC strength (b) Stirrups strength

(c) Steel strength (d) Steel ratio

Fig. 11 Influence rules of parameters on hysteresis loops of SRRC columns

evaluate the ductility of columns. In the equation, Δ_u and Δ_y are the displacements of column that correspond to its ultimate load and yield load, respectively.

From Table 5, the influence of analysis parameters on the bearing capacity and ductility of SRRC columns can be described as follow:

(1) The peak loads of SRRC13 and SRRC13-2 were about higher than that of SRRC13-1 by 3.62% and 10.08%, respectively. It shows that the horizontal bearing capacity and stiffness of columns can be improved by the increasing RAC strength. On the contrary, compared with SRRC13-1 column, the ductility factors of SRRC13 and SRRC13-2 decreased by 4.87% and 9.46%, respectively. It indicates that the ductility of SRRC columns was unfavourably influenced by the increasing RAC strength.

(2) Compared with SRRC13-2 using HRB335, the horizontal bearing capacity of columns using HRB400 and HRB500 increased by 2.95% and 3.65%, respectively. In addition, the ductility factors of columns using HRB400 and HRB500 also increased by 3.91% and 9.64% than that of SRRC13-2, respectively. It indicates that the stirrups strength has favorable effect on the bearing capacity and ductility of columns but that such effect was not obvious.

(3) Compared with SRRC columns using Q235, the bearing capacity of columns using Q345 and Q390 increased by 15.78% and 20.6%, respectively. Meanwhile, the ductility factors of columns using Q345 and Q390 increased by 6.02% and 9.94% than that of HRB335, respectively. Obviously, the bearing capacity and ductility of SRRC columns can be

Table 5 Bearing capacity and ductility factors of parameters analysis of SRRC columns

Columns No.	RAC strength	Stirrups strength	Steel strength	Steel ratio	Horizontal bearing capacity / kN	Ductility factors
SRRC13	C40	HRB335	Q235	4.98%	149.30	3.32
SRRC13-1	C30	HRB335	Q235	4.98%	144.08	3.49
SRRC13-2	C50	HRB335	Q235	4.98%	158.60	3.16
SRRC13-3	C40	HRB400	Q235	4.98%	153.70	3.45
SRRC13-4	C40	HRB500	Q235	4.98%	154.75	3.64
SRRC13-5	C40	HRB335	Q345	4.98%	172.86	3.52
SRRC13-6	C40	HRB335	Q390	4.98%	180.06	3.65
SRRC13-7	C40	HRB335	Q235	4.19%	137.29	3.02
SRRC13-8	C40	HRB335	Q235	6.04%	170.01	4.13

improved by the increasing of steel strength.

(4) The bearing capacity and ductility of SRRC columns increase obviously with the increasing steel ratio. Based on Table 5, compared with SRRC13-7, the peak loads of SRRC13 and SRRC13-8 were about higher than those of SRRC13-7 by 8.75% and 23.83%, respectively. In addition, the ductility factors of SRRC13 and SRRC13-8 increased by 9.93% and 36.75% than that of SRRC13-7, respectively. It indicates that the increase of steel ratio can considerably improved the ductility of SRRC columns.

More importantly, the ductility factors of parameters analysis of SRRC columns were greater than 3.0, which indicate that the columns is high ductility under cycle loads through the reasonable design. It means that SRRC column suffered from flexure failure has good seismic performance.

5. Horizontal bearing capacity of SRRC columns

5.1 Flexural failure mechanism of SRRC columns

Based on the above analysis, SRRC columns possessing a large shear span ratio (i.e., $\lambda \geq 2.0$) were usually suffered from typical flexural failure under lateral cycle loads. In this paper, SRRC13 column was taken as an example for the analysis of flexural failure mechanism. Fig. 12 presents the strain characteristics of the stirrups, longitudinal reinforcements, steel flanges and steel web of SRRC13 column. As shown in Fig. 12 and Table 2, after the peak load of column reached, the longitudinal reinforcements and steel flanges of SRRC13 column had yielded thoroughly, whereas the transverse stirrups and steel web did not yield completely. This finding shows that the bending deformation of column plays the decisive role in its failure process, while the shear deformation of columns can almost be ignored because the shear deformation was not obvious.

In fact, according to the test results, many transverse cracks at the bottom of SRRC columns linked together and penetrated completely before failure, which can be classified as a typical phenomenon of flexural failure. As the increase of lateral cycle loads, the plastic hinge was observed in the bottom of SRRC columns, as shown Figs. 13(a)-(c). After the columns reached the peak loads, more and more RAC cover at the bottom of SRRC columns falling off seriously, the

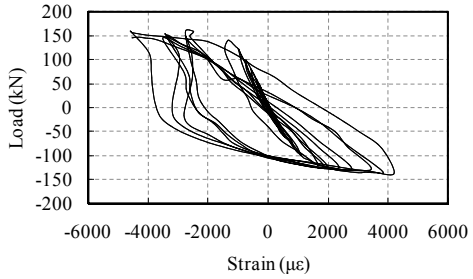

(a) Strain characteristics of longitudinal rebars

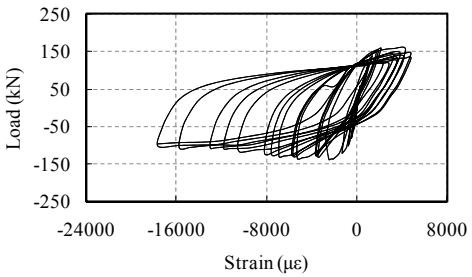

(b) Strain characteristics of steel flanges

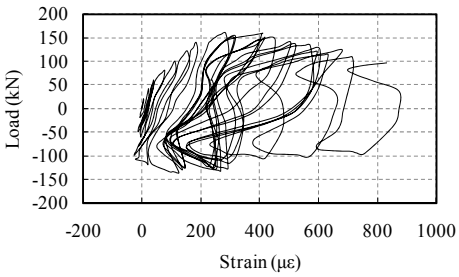

(c) Strain characteristics of stirrups

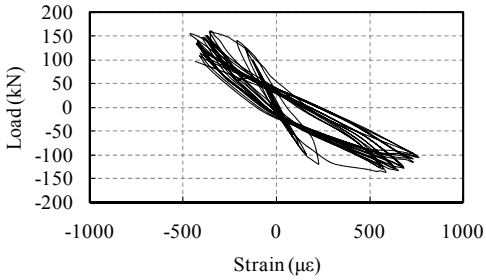

(d) Strain characteristics of steel web

Fig. 12 Strain characteristics of steel material in SRRC13 column

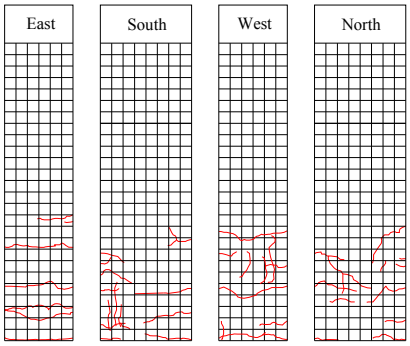

(a) Crack distribution of SRRC13

(b) Flexural failure of SRRC13

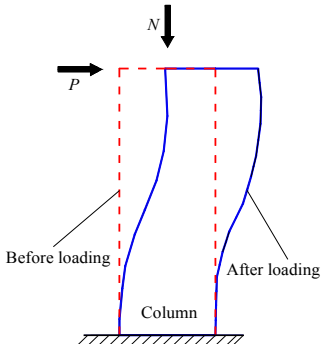

(c) Bending deformation of coulmns

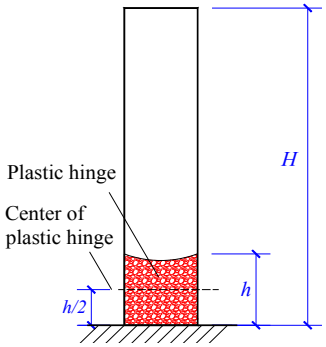

(d) Plastic hinge in columns

Fig. 13 Failure characteristics and plastic hinge of SRRC columns

longitudinal rebars and steel yielded absolutely due to the pressure. Meanwhile, the resisting force of SRRC columns dropped rapidly, which means that the columns have lost their bearing capacity. It can be summarized as flexural failure.

In the above analysis, SRRC columns were suffered to the vertical axial force under lateral cyclic loads. As a result, the bending moment of columns produced by the combined action of lateral loads and vertical axial loads was gradually increasing as the increase of the loads. The bending moment of the bottom of columns is greater than other parts, which shows that the bottom of columns is firstly destroyed under lateral cyclic loads. It leads to that the plastic hinge was produced at the bottom of columns. It suggests the bending moment of the cross section of SRRC column bottom is able to determine the horizontal bearing capacity of columns, which means that the flexural failure characteristics of SRRC columns under lateral cyclic loads are similar to the failure characteristics of the normal section of eccentrically loaded columns. Therefore, the horizontal bearing capacity of SRRC columns under lateral cyclic loads depends mainly on the flexural bearing capacity of normal section of columns.

5.2 Calculation of horizontal bearing capacity for SRRC columns

5.2.1 Nominal moment capacity of SRRC columns

The computing theories of flexural bearing capacity of normal section for the eccentrically loaded SRRC columns was summarized and put forward in the literatures (Cui 2011, Chen *et al*. 2014). Therefore, the bending strength of SRRC columns suffered to the axial force under lateral loads can be calculated according to the formulas of the eccentrically loaded SRRC columns. The failure modes of normal-section compression in the eccentrically loaded SRRC columns can be divided into the small eccentric compression failure and the large eccentric compression failure. The typical failure features of the small eccentric compression columns can be describe as: the compressive RAC of columns crushed before the steel flange yielded, which belongs to brittle failure. While the failure features of the large eccentric compression columns shows the steel flange can be able to yield when the compressive RAC of columns crushed seriously, which belongs to ductile failure. According to the test results, the steel flanges of all the SRRC columns yielded completely based on chapter 5.1, which conforms to the failure characteristics of the large eccentric compression columns. It indicates that the flexural failures of SRRC columns under lateral loads belong to the large eccentric compression failure.

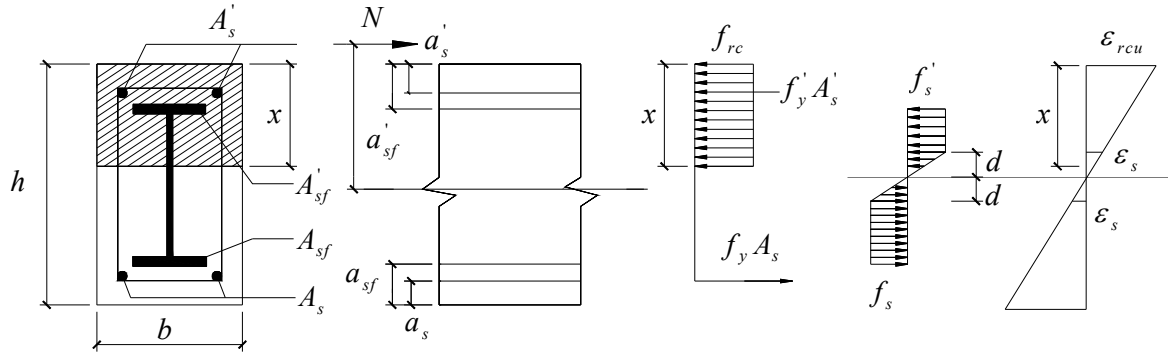

Fig. 14 Force diagram of the large eccentric compression SRRC columns

Based on the above analysis, Fig. 14 shows the force diagram and strain distribution of the normal section of SRRC columns which suffered from the large eccentric compression failure. From Fig. 14, when SRRC columns suffered from the large eccentric compression failure, RAC in the compression zone of normal section reached ultimate compressive strain and crushed, while the steel flanges in the tension zone of columns had also achieved to its yield strength. Before the failure of SRRC columns, the cross-section strain distribution along the height of the normal section is almost linear, which indicates the plane-section assumption was established in the normal section of SRRC columns. Besides, the tensile properties of RAC in the tension zone can be ignored. Based on the above analysis, the nominal moment capacity of SRRC columns under lateral loads can be calculated by the basic Eqs. (7)-(10).

From Fig. 14, the basic formulas of bearing capacity of the large eccentric compression SRRC columns can be established through the force and moment balance theory.

The force balance equation of cross-section of SRRC columns can be expressed by

$$\begin{aligned} N = {} & f_{rc} bx + f_y^{'} A_s^{'} + f_s^{'} A_{sf}^{'} + f_s^{'} \left(1.25x - a_{sf}^{'} - d\right) t_w \\ & - f_y A_s - f_s A_{sf} - f_s \left(h - a_s - 1.25x - d\right) t_w \end{aligned} \tag{7}$$

The moment balance equation for the neutral axis of the cross-section of SRRC column can be established by

$$\begin{aligned} M = {} & \frac{1}{2} f_{rc} bx^2 + f_y^{'} A_s^{'} \left(x - a_s^{'}\right) + f_y A_s \left(h - a_s - x\right) \\ & + f_s A_{sf}^{'} \left(x - a_{sf}^{'}\right) + f_s A_{sf} \left(h - a_{sf} - x\right) + \frac{1}{2} f_s h_s^2 t_w - \frac{2}{3} f_s d^2 t_w \end{aligned} \tag{8}$$

$$d = \frac{f_s x}{0.8 \varepsilon_{rcu} E_s} \tag{9}$$

$$x \leqslant x_b = \xi_b h_0 = \frac{0.8}{1 + \dfrac{f_s}{E_s \varepsilon_{rcu}}} h_0 \tag{10}$$

Where d is the height of the unyielding steel web in the cross-section of SRRC columns and x is the compression height of the cross-section of columns. In addition, x_b is the ultimate compression height of the cross-section of SRRC columns, which can be used to determine the small or large eccentric compression columns. 0.8 is the coefficient of the equivalent rectangular stress block for the compression zone of RAC in the cross-section section of columns. Other symbols in Eqs. (7) to (10) have been defined in symbol table in this paper. The detailed analysis of Eqs. (7) to (10) of the nominal moment capacity of SRRC columns can be seen in the literature (Cui 2011, Chen *et al*. 2014).

5.2.2 Nominal horizontal bearing capacity of SRRC columns

Obviously, the bending moment of the neighborhood of SRRC column' bottom is greater than its other parts, which produced by the combined action of horizontal loads and vertical loads. As a result, the plastic hinge can be observed in the bottom of SRRC columns. Therefore, the influence of plastic hinge region on the tested moment strength of columns must be taken into account (Zhou

and Liu 2010, ACI Committee 2011). Based on the test results, the height of plastic hinge region of SRRC columns can be about h, as shown Fig. 13(d). Therefore, the normal moment strength of the cross section of SRRC columns' bottom can be calculated by the following equation

$$M = p_{cu}\left(H - \frac{h}{2}\right) + N\Delta_u \tag{11}$$

Where H is the height of SRRC columns; h is the height of the section of columns; P_{cu} is the calculated nominal horizontal bearing capacity of columns; and Δ_u is the ultimate displacement of columns.

In fact, the influence of Δ_u on the moment strength M of SRRC columns is relatively small. Therefore, the influence of Δ_u can be ignored so as to simplify the calculation process. According to the Eq. (11), the nominal horizontal bearing capacity of SRRC columns can be expressed by the following formula

$$p_{cu} = \frac{M}{H - h/2} \tag{12}$$

Comparison results among the test values, numerical values and calculated values based on the proposed methods are listed in Table 6, where p_{cu} is the nominal horizontal bearing capacity of SRRC columns adopting the proposed formulas in this paper. From Table 6, the predictions agree well with the test results of the SRRC columns. Therefore, the proposed formulas can be adopted

Table 6 Comparisons among the test values, numerical values and calculated values

Specimen No.	P_t / kN	P_{cu} / kN	P_{cu} / P_t
SRRC9	283.6	305.1	1.076
SRRC10	224.8	222.8	0.991
SRRC11	146.9	150.3	1.023
SRRC12	154.6	149.9	0.970
SRRC13	147.5	150.2	1.018
SRRC14	135.7	130.0	0.958
SRRC15	168.9	184.4	1.091
SRRC16	142.4	150.2	1.055
SRRC17	158.3	149.7	0.946
Specimen No.	P_t / kN	P_{cu} / kN	P_{cu} / P_t
SRRC13-1	144.1	150.3	1.044
SRRC13-2	158.6	147.9	0.933
SRRC13-3	153.7	150.2	0.977
SRRC13-4	154.8	150.2	0.971
SRRC13-5	172.9	160.5	0.928
SRRC13-6	180.1	170.1	0.945
SRRC13-7	137.3	139.5	1.016
SRRC13-8	170.0	167.1	0.983

to evaluate the nominal horizontal bearing capacity of SRRC columns, which suffers from flexural failure under cyclic loads.

6. Conclusions

The researches on numerical analysis and horizontal bearing capacity of SRRC columns under cyclic loads were performed in this paper. The following conclusions can be made based on the analysis results:

(1) The calculated hysteresis loops of SRRC columns using OpenSees software is almost the same as the shape of test curves based on the reasonable models. Most of the calculated bearing capacity of columns is greater than the test values. The main reasons may be that the shear deformation of columns and the effect of the bond-slip between profile steel and RAC are ignored completely in this analysis.
(2) The parameter analysis shows that all the hysteresis loops of columns are homogeneous symmetric and plump, which reflects that SRRC columns have excellent ductility and energy dissipation capacity, especially under some beneficial design parameters.
(3) It shows that the increasing RAC strength has an unfavourable influence on the ductile deformation of SRRC columns. While the bearing capacity of columns increase as the increase of RAC strength.
(4) The bearing capacity and ductility of columns increase a little as the increase of stirrups strength. It indicates that the effect of stirrups strength on the bearing capacity and ductility of SRRC columns was not obvious.
(5) The seismic performance (e.g., the horizontal bearing capacity, ductility) of SRRC columns can be improved obviously through the increase of steel strength and steel ratio.
(6) Based on the computing theories of normal section of bearing capacity for the eccentrically loaded columns, the calculation formulas of nominal horizontal bearing capacity of SRRC columns were proposed. The calculation results according to the proposed formulas of columns agreed with the test results. However, further investigations must be performed to verify the effectiveness of design method.

Acknowledgments

The research described in this paper was financially supported by the National Natural Science Foundation of China P.R. (No. 51408485 and 51178384), China Postdoctoral Science Foundation Funded Project (No. 2015M572584), the Plan Projects of the Ministry of Housing and Urban-rural Development of China P.R. (No. 2015-K2-011), Young Talent Fund of University Association for Science and Technology in Shaanxi of China. (No. 20150114), the Project Supported by Natural Science Basic Research Plan in Shaanxi Province of China (No. 2016JQ5024), which is gratefully acknowledged.

References

ACI Committee (2011), American Concrete Institute and International Organization for Standardization; Building code requirements for structural concrete (ACI 318-11) and commentary, American Concrete

Institute.
Chen, Z.P., Zhong, M., Chen, Y.L., Xue, J.Y. and Cui, W.G. (2014), "Mechanical behavior and computed bearing capacity of steel reinforced recycled aggregate concrete columns under eccentric loading", *Eng. Mech.*, **31**(4), 160-170.
Chen, Z.P., Xu, J.J., Chen, Y.L. and Xue, J.Y. (2015), "Seismic behavior of steel reinforced concrete (SRC) T-shaped column-beam planar and 3D hybrid joints under cyclic loads", *Earthq. Struct., Int. J.*, **8**(3), 555-572.
Chitawadagi, M.V., Narasimhan, M.C. and Kulkarni, S.M. (2010), "Axial strength of circular concrete-filled steel tube columns – DOE approach", *J. Constr. Steel. Res.*, **66**(10), 1248-1260.
Cui, W.G. (2011), "Experimental study on mechanical behaviors of normal cross-section of steel reinforced recycled concrete composite columns", Master Thesis; Xi'an University of Architecture and Technology.
Denavit, M.D. and Hajjar, J.F. (2014), "Characterization of behavior of steel-concrete composite members and frames with applications for design", Newmark Structural Engineering Laboratory, University of Illinois at Urbana-Champaign.
Fathifazl, G., Abbas, A., Razaqpur, A.G., Isgor, O.B., Fournier, B. and Foo, S. (2009a), "New mixture proportioning method for concrete made with coarse recycled concrete aggregate", *J. Mater. Civil. Eng.*, **21**(10), 601-611.
Fathifazl, G., Razaqpur, A.G., Isgor, O.B., Abbas, A., Fournier, B. and Foo, S. (2009b), "Flexural performance of steel-reinforced recycled concrete beams", *ACI Struct. J.*, **106**(6), 858-867.
Fathifazl, G., Razaqpur, A.G., Isgor, O.B., Abbasd, A., Fourniere, B. and Foof, S. (2011), "Shear capacity evaluation of steel reinforced recycled concrete (RRC) beams", *Eng. Struct.*, **33**(3), 1025-1033.
Gonzalez, V.C.L. and Moriconi, G. (2014), "The influence of recycled concrete aggregates on the behavior of beam–column joints under cyclic loading", *Eng. Struct.*, **60**(2),148-154.
Hassanein, M.F., Kharoob, O.F. and Gardner, L. (2015), "Behaviour and design of square concrete-filled double skin tubular columns with inner circular tubes", *Eng. Struct.*, **100**(10), 410-424.
Huang, Y.J., Xiao, J.Z. and Zhang, C.H. (2012), "Theoretical study on mechanical behavior of steel confined recycled aggregate concrete", *J. Constr. Steel. Res.*, **76**(9), 100-111.
Kang, H.Z., Song, X.M., Jia, K.W., Zhou, L.P. and Liu, P. (2013), "Numerical analyses on seismic behaviour of concrete-filled steel tube composite columns based on OpenSEES program", *J. Eng. Sci. Tech. Rev.*, **6**(5), 143-148.
Kim, S.W. and Yun, H.D. (2013), "Influence of recycled coarse aggregates on the bond behavior of deformed bars in concrete", *Eng. Struct.*, **48**(3), 133-143.
Kim, S.H., Jung, C.Y. and Ann, J.H. (2011), "Ultimate strength of composite structure with different degrees of shear connection", *Steel Compos. Struct., Int. J.*, **11**(5), 375-390.
Li, X.P. (2008), "Recycling and reuse of waste concrete in China: Part I. Material behaviour of recycled aggregate concrete", *Resour. Conserv. Recy.*, **53**(1-2), 36-44.
Li, X.P. (2009), "Recycling and reuse of waste concrete in China: Part II. Structural behaviour of recycled aggregate concrete and engineering applications", *Resour. Conserv. Recy.*, **53**(1), 107-112.
Li, W., Li, Q.N. and Jiang, W.S. (2012), "Parameter study on composite frames consisting of steel beams and reinforced concrete columns", *J. Constr. Steel. Res.*, **77**(10), 145-162.
Li, W.G., Xiao, J.Z., Shi, C.J. and Poon, C.S. (2015), "Structural behaviour of composite members with recycled aggregate concrete-an overview", *Adv. Struct. Eng.*, **18**(6), 919-938.
Lu, X.Z., Xie, L.L., Guan, H. and Lu, X. (2015), "A shear wall element for nonlinear seismic analysis of super-tall buildings using OpenSees", *Finite Elem. Anal. Des.*, **98**(6), 14-25.
Ma, H., Xue, J.Y., Zhang, X.C. and Luo, D.M. (2013), "Seismic performance of steel-reinforced recycled concrete columns under low cyclic loads", *Constr. Build. Mater.*, **48**(11), 229-237.
Ma, H., Xue, J.Y., Liu, Y.H. and Zhang, X.C. (2015), "Cyclic loading tests and shear strength of steel reinforced recycled concrete short columns", *Eng. Struct.*, **92**(6), 55-68.
Mazzoni, S., Mckenna, F., Scott, M.H. and Fenves, G.L. (2006), "OpenSees command language manual", Pacific Earthquake Engineering Research (PEER) Center.
Moridani, K.K. and Zarfam, P. (2013), "Nonlinear analysis of reinforced concrete joints with bond-slip

effect consideration in OpenSees", *Nonlinear Anal*., **3**(6), 362-367.
Tabsh, S.W. and Abdelfatah, A.S. (2009), "Influence of recycled concrete aggregates on strength properties of concrete", *Constr*. *Build*. *Mater*., **23**(2), 1163-1167.
Talaeitaba, S.B., Halabian, M. and Torki, M.E. (2015), "Nonlinear behavior of FRP-reinforced concrete-filled double-skin tubular columns using finite element analysis", *Thin*. *Wall*. *Struct*., **95**(10), 389-407.
Thomas, C., Setién, J., Polanco, J.A., Alaejos, P. and Juanb, M.S.d. (2013), "Durability of recycled aggregate concrete", *Constr*. *Build*. *Mater*., **40**(3), 1054-1065
Wang, Y.Y., Chen, J. and Geng, Y. (2015a), "Testing and analysis of axially loaded normal-strength recycled aggregate concrete filled steel tubular stub columns", *Eng*. *Struct*., **86**(3), 192-212.
Wang, Q.W, Shi, Q.X and Tian, H.H. (2015b), "Seismic behavior of steel reinforced concrete (SRC) joints with new-type section steel under cyclic loading", *Steel Compos*. *Struct*., *Int*. *J*., **19**(6), 1561-1580
Won, C.C. and Hyun, D.Y. (2012), "Compressive behavior of reinforced concrete columns with recycled aggregate under uniaxial loading", *Eng*. *Struct*., **41**(8), 285-293.
Xiao, J.Z., Li, W.G., Fan, Y.H. and Huang, X. (2012a), "An overview of study on recycled aggregate concrete in China (1996–2011)", *Constr*. *Build*. *Mater*., **31**(6), 364-383.
Xiao, J.Z., Huang, X. and Shen, L.M. (2012b), "Seismic behavior of semi-precast column with recycled aggregate concrete", *Constr*. *Build*. *Mater*., **35**(10), 988-1001.
Xue, J.Y., Chen, Z.P., Zhao, H.T., Gao, L. and Liu, Z.Q. (2012), "Shear mechanism and bearing capacity calculation on steel reinforced concrete special-shaped columns", *Steel Compos*. *Struct*., *Int*. *J*., **13**(5), 473-487.
Zhou, X.H. and Liu, J.P. (2010), "Seismic behavior and strength of tubed steel reinforced concrete (SRC) short columns", *J*. *Constr*. *Steel*. *Res*., **66**(7), 885-896.

CC

Nomenclature

H	the height of SRRC columns;	P	the horizontal loads;
b	the width of the section of SRRC columns;	N	the vertical axial loads;
h	the height of the section of SRRC columns;	f_{rc}	the design strength of RAC;
r	RCA replacement percentage;	x	the compression height of the cross section of column;
λ	shear span ratio;	$f_y^{'}$	the yield strength of longitudinal rebars under compression;
n	axial compression ratio;	$A_s^{'}$	the cross sectional area of longitudinal rebars in compression;
ρ_s	stirrups ratio;	$f_s^{'}$	the yield strength of steel flanges in compression;
f_{rcu}	the cube compressive strength of RAC;	$A_{sf}^{'}$	the cross sectional area of steel flanges in compression;
E_{rc}	the modulus of elasticity of RAC;	$a_{sf}^{'}$	the vertical distance from the center of compression steel flange to the edge of cross section;
σ_c, ε_c	the stress and strain of concrete, respectively;	d	the height of the unyielding steel web in the cross section of columns;
K	the enhancement coefficient of concrete strength due to the steel rebar skeleton;	t_w	the thickness of steel web;
ε_0	the peak strain of concrete;	f_y	the yield strength of longitudinal rebars in tension;
f_c	the design compressive strength of concrete;	A_s	the cross sectional area of longitudinal rebars in tension;
Z_m	the slope of softening section in concrete 01 model;	f_s	the yield strength of steel flanges in tension;
f_{yh}	the strength of stirrups;	A_{sf}	the cross sectional area of steel flanges in tension;
s_h	the spacing of stirrups;	a_s	the vertical distance from the center of tension longitudinal rebars to the edge of cross section;
h_c	the width of core concrete surrounded by stirrups;	a_{sf}	the vertical distance from the center of tension steel flange to the edge of cross section;
ε_u	the ultimate strain of concrete;	h_s	the height of the section of steel web;
R_0	the nonlinear transition value from elastic stage to strain hardening stage of steel;	ε_{rcu}	the ultimate strain of RAC;

b_1	the strain hardening rate of steel bars;	E_s	the modulus of elasticity of steel material;
C_{R2},C_{R1}	the control coefficient of the curve shape of Steel02 model;	M	the moment strength of cross section of columns;
P_t	the test values of horizontal bearing capacity of columns;	h_0	Effective height of the section of rectangular columns;
P_n	the numerical values of horizontal bearing capacity of columns;	x_b	the ultimate compression height of the cross section of columns;
δ	the calculation error;	ξ_b	the relative depth of limiting compression zone of cross section of columns;
μ	the ductility factor;	h_0	the effective height of cross section;
Δ_y, Δ_u	the yield displacement and ultimate displacement of columns , respectively;	P_{cu}	the calculated values of horizontal bearing capacity;